

# Discrete Glimpses

of the Physics Landscape after the Higgs Discovery

**John Ellis**

Physics Department, King's College London, Strand, London WC2R 2LS, U.K; Theory Division, Physics Department, CERN, CH 1211 Geneva 23, Switzerland

E-mail: [John.Ellis@cern.ch](mailto:John.Ellis@cern.ch)

**Abstract.** What is the Higgs boson telling us? What else is there? How do we find it? This talk discusses these current topics in particle physics in the wake of the Higgs discovery, with particular emphasis on the discrete symmetries CP and R-parity, not forgetting flavour physics and dark matter, and finishing with some remarks about possible future colliders.

KCL-PH-TH/2015-02, LCTS/2015-01, CERN-PH-TH/2015-008

## 1. The Story so far

Run 1 of the LHC has brought the apotheosis of the Standard Model (SM). The SM has predicted successfully many cross sections for particle and jet production measured at the LHC [1], as seen in Fig. 1. These successes include QCD jet production cross sections, which agree with SM predictions over large ranges in energy and many orders of magnitude, measurements of single and multiple  $W^\pm$  and  $Z^0$  production, as well as multiple measurements of top quark production, both pairwise and singly and in association with vector bosons. Moreover, Run 1 of the LHC has also brought the discovery by CMS and ATLAS of a (the?) Higgs boson [2], whose production has by now been observed in three different production channels, as also seen in Fig. 1, again with cross sections in agreement with the SM predictions. A major theme of this talk is what we already know about this newly-discovered particle.

Meanwhile, over there in flavour space, the Cabibbo-Kobayashi-Maskawa (CKM) description of flavour mixing and CP violation is also a pillar of the SM, but here the picture is more complex. It is in general very successful, as seen in the left panel of Fig. 2 [3], but there are a number of anomalies. On the one hand, the SM predicted successfully the branching ratio for the rare decay  $B_s \rightarrow \mu^+ \mu^-$ :

$$BR(B_s \rightarrow \mu^+ \mu^-) = 2.8_{-0.6}^{+0.7} \times 10^{-9}, \quad (1)$$

measured by the CMS and LHCb Collaborations [4]: see Fig. 3. However, the joint CMS and LHCb analysis [4] also has a suggestion of a  $B_d \rightarrow \mu^+ \mu^-$  signal that is considerably larger than the SM prediction (which is an ironclad prediction also of models with minimal flavour violation (MFV), including many SUSY scenarios):

$$BR(B_d \rightarrow \mu^+ \mu^-) = 3.9_{-1.4}^{+1.6} \times 10^{-10}, \quad (2)$$



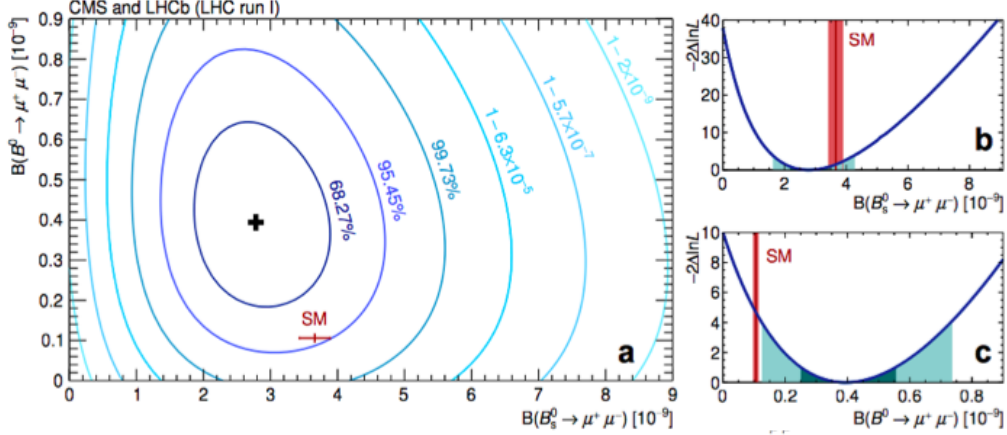


**Figure 3.** Panel **a**: measurements by the CMS and LHCb Collaborations [4] of  $B_{s,d} \rightarrow \mu^+ \mu^-$  decays. Panel **b**: The CMS and LHCb Collaborations see a clear signal for  $B_s \rightarrow \mu^+ \mu^-$  decay. Panel **c**: They also see a possible hint of  $B_d \rightarrow \mu^+ \mu^-$  decay.

diimuon asymmetry at the Tevatron [8]. On the other hand, some anomalies do seem to be going away, such as the forward-backward asymmetry in  $t\bar{t}$  production, which now agrees with higher-order QCD calculations [9], as does the  $t\bar{t}$  rapidity asymmetry measured at the LHC. However, the discrete charm of flavour physics leaves many issues to be addressed during LHC Run 2 and at SuperKEK-B.

One of the principal focuses during Run 2 of the LHC will be the more detailed study of the Higgs boson and probes whether its properties deviate from SM predictions, e.g., in the flavour sector. As I discuss later, the measurement of the Higgs mass has produced new reasons to expect BSM physics, and the search for BSM physics will start anew at Run 2, with its greatly increased centre-of-mass energy and increased integrated luminosity. My personal favourite candidate for BSM physics is supersymmetry (SUSY), and I also discuss later in this talk how SUSY models are constrained by flavour physics, as well as by the observations to date of the Higgs boson and searches for BSM physics with Run-1 data. This talk concludes with some remarks about searches for particle dark matter at the LHC and elsewhere, and some advertisements for possible future colliders.

## 2. Higgs Physics

### 2.1. Mass Measurements

The mass of the Higgs boson can be measured most accurately in the  $\gamma\gamma$  and  $ZZ^* \rightarrow 2\ell^+ 2\ell^-$  final states, and ATLAS and CMS both report accurate measurements in both these final states. ATLAS measures [10]

$$\text{ATLAS combined : } m_H = 125.36 \pm 0.37 \pm 0.18 \text{ GeV} = 125.36 \pm 0.41 \text{ GeV}, \quad (3)$$

and CMS measures [11]

$$\text{CMS combined : } m_H = 125.03^{+0.26}_{-0.27} {}^{+0.13}_{-0.15} \text{ GeV} = 125.03 \pm 0.30 \text{ GeV}. \quad (4)$$

Some interest has been generated by the differences in the masses measured in these channels, but these have opposite signs in the two experiments:

$$\begin{aligned} \text{ATLAS : } \Delta m_H &= 1.47 \pm 0.67 \pm 0.18 \text{ GeV}, \\ \text{CMS : } \Delta m_H &= -0.9 \pm 0.4 \pm 0.2^{+0.34}_{-0.35} \text{ GeV}, \end{aligned} \quad (5)$$

so are presumably statistical and/or systematic artefacts. Combining naively the ATLAS and CMS measurements yields

$$m_H = 125.15 \pm 0.24 \text{ GeV}. \quad (6)$$

In addition to being a fundamental measurement in its own right, and casting light on the possible validity of various BSM models, the precise value of  $m_H$  is also important for the stability of the electroweak vacuum in the Standard Model, as discussed later.

## 2.2. The Higgs Spin and Parity

The fact that the Higgs boson has been observed to decay into  $\gamma\gamma$  excludes spin 1, and spin 0 is expected, but spins 2 and higher are also possible in principle. There have been many probes of the Higgs spin [12, 13, 14], including its production and decay rates [15], the kinematics of its production in association with massive vector bosons [16], as well as angular distributions in its decays into  $W^+W^-$ ,  $ZZ$  and  $\gamma\gamma$  [17]. The results of many of these tests are shown in Fig. 4. By now there is overwhelming evidence that the Higgs boson has spin 0 and that its couplings to  $W^+W^-$  and  $ZZ$  are predominantly CP-even.

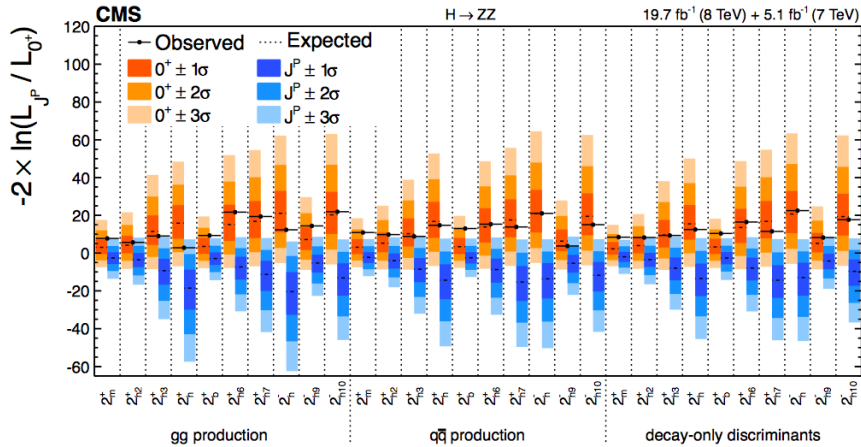


**Figure 4.** Tests of spin-parity hypotheses for the Higgs boson. All favour strongly the  $0^+$  assignment expected in the SM [13].

On the other hand, it is possible that there may be an admixture of CP-odd couplings, and their fraction may depend on the particle whose coupling to the Higgs boson are being probed. In particular, the leading CP-odd  $H$  coupling to fermions would have the *same* (zero) dimension as the leading CP-even coupling, whereas the leading CP-odd  $H$  coupling to massive vector bosons would have *higher* dimension than the leading CP-even coupling, so it may be more suppressed. Various ways to probe CP violation in the  $H\tau^+\tau^-$  couplings have been proposed [18], and it is also possible to probe CP violation in the  $Ht\bar{t}$  couplings [19]. These would affect the total cross sections for associated  $Ht\bar{t}$ ,  $Ht$  and  $H\bar{t}$  production, as seen in the left panel of Fig. 5 as functions of  $\zeta_t \equiv \arctan(\text{CP-odd coupling}/\text{CP-even coupling})$ . If  $\zeta_t \neq 0$ , a CP-violating transverse polarization asymmetry is in principle observable in  $Ht$  and  $H\bar{t}$  production, as shown in the right panel of Fig. 5.

## 2.3. Higgs Couplings

As seen in Fig. 6, the strengths of the Higgs signals measured by ATLAS and CMS individual channels are generally compatible with the SM predictions within the statistical fluctuations [20, 21, 11], which are inevitably large at this stage. Combining their measurements

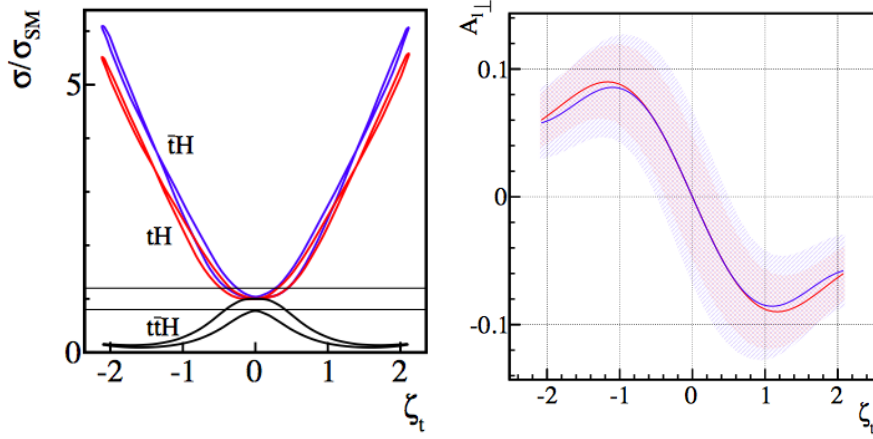


**Figure 5.** Left panel: The effects of a CP-violating coupling on the  $Ht\bar{t}$ ,  $Ht$  and  $H\bar{t}$  production cross sections. Right panel: A CP-violating transverse polarization asymmetry observable in  $Ht$  and  $H\bar{t}$  production [19].

in the  $\gamma\gamma$ ,  $ZZ^*$ ,  $WW^*$ ,  $b\bar{b}$  and  $\tau^+\tau^-$  channels, ATLAS and CMS report the following overall signal strengths:

$$\begin{aligned} \text{ATLAS : } \mu &= 1.30 \pm 0.12 \pm 0.10 \pm 0.09, \\ \text{CMS : } \mu &= 1.00 \pm 0.09 \stackrel{+0.08}{-0.07} \pm 0.07. \end{aligned} \quad (7)$$

These averages are again quite compatible with each other and with the SM, and measurements at the Tevatron are also compatible with SM predictions for the Higgs boson [22].

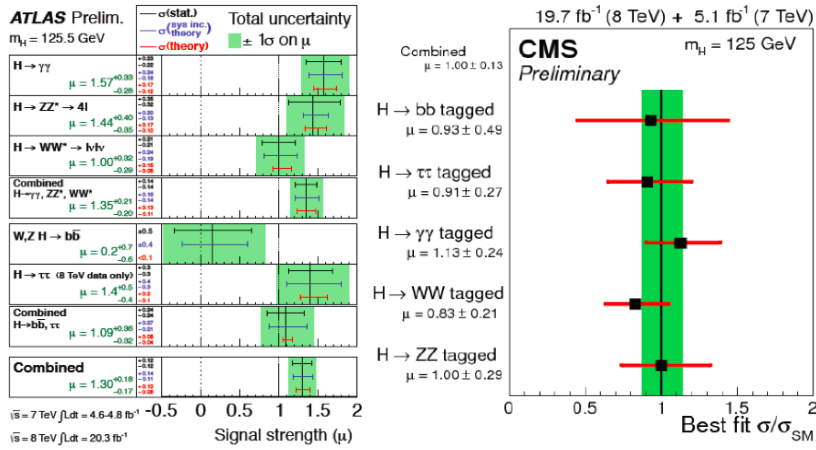


**Figure 6.** The Higgs signal strengths  $\mu$ , normalised to unity for the SM, as measured by ATLAS [20] (left panel) and CMS [11] (right panel).

One distinctive feature of the Higgs couplings to other particles in the SM is that they should be related to their masses: linearly for fermions, quadratically for bosons, and be proportional to the Higgs vev  $v = 246$  GeV. These predictions are verified indirectly by the measurements in Fig. 6, but one may also test these predictions directly, as seen in Fig. 7. This shows the result

of a global fit to the data parametrising the Higgs couplings as [23]

$$\lambda_f = \sqrt{2} \left( \frac{m_f}{M} \right)^{(1+\epsilon)}, \quad g_V = 2 \left( \frac{M_V^{2(1+\epsilon)}}{M^{(1+\epsilon)}} \right). \quad (8)$$

As seen in the left panel of Fig. 7, the data yielded

$$\epsilon = -0.022^{+0.020}_{-0.043}, \quad M = 244^{+20}_{-10} \text{ GeV}, \quad (9)$$

quite compatible with the SM predictions  $\epsilon = 0$ ,  $M = 246$  GeV. Similar results have also been found recently in an analysis by the CMS Collaboration [21]. It seems that Higgs couplings have a very similar flavour structure to particle masses.

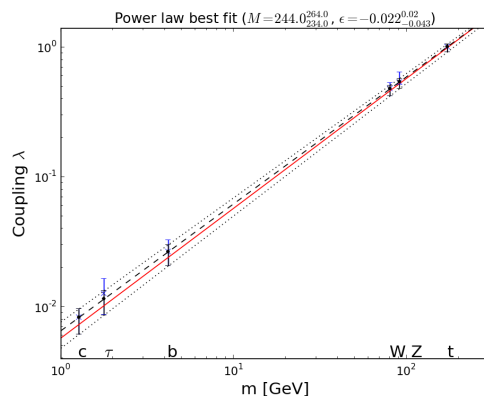


**Figure 7.** A global fit to the  $H$  couplings of the form (8) (central values as dashed and  $\pm 1\sigma$  values as dotted lines), which is very compatible with the expected linear mass dependence for fermions and quadratic mass dependence for bosons (solid red line) [23].

A related aspect of the SM is the expectation is that flavour should be conserved to a very good approximation in Higgs couplings to fermions. This is indeed consistent with the upper limits on low-energy effective flavour-changing interactions, but these would allow also lepton-flavour-violating Higgs couplings much larger than the SM predictions, so looking for such interactions is a possible window on BSM physics. We estimated on the basis of low-energy data that the branching ratios for  $H \rightarrow \mu\tau$  and  $H \rightarrow e\tau$  decays could each be as large as  $\mathcal{O}(10)\%$ , i.e., as large as  $\text{BR}(H \rightarrow \tau\tau)$ , whereas the branching ratio for  $H \rightarrow \mu e$  could only be  $\lesssim 10^{-5}$  [24]. The CMS Collaboration has recently found [7]

$$\text{BR}(H \rightarrow \mu\tau) = 0.89^{+0.40}_{-0.37} \%, \quad (10)$$

corresponding to a background-only  $p$ -value of 0.007, a  $\sim 2.46\sigma$  effect. LHC Higgs measurements are therefore already testing SM flavour physics predictions more stringently than previous low-energy experiments, and we are on tenterhooks to see corresponding results from ATLAS and from Run 2 of the LHC!

With the discovery of the Higgs boson at the LHC, one of the key questions was whether it is elementary or composite. It used to be thought that a composite Higgs boson would normally have a mass comparable to the scale of compositeness, but this can be reduced if it is a pseudo-Nambu-Goldstone boson whose mass is protected by some approximate symmetry, possibly compatible with the measured Higgs mass  $\sim 125$  GeV. The compositeness possibility may be

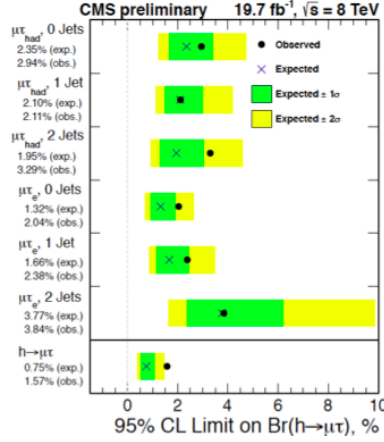


**Figure 8.** Results from the CMS search for  $H \rightarrow \mu\tau$  decay [7].

probed using a phenomenological Lagrangian  $\mathcal{L}$  with free parameters to describe  $H$  interactions, that may be constrained using  $H$  production and decay data. In view of the consistency of the Standard Model relation  $\rho \equiv m_W/m_Z \cos \theta_W = 1$  with data, one may assume a custodial symmetry in this phenomenological Lagrangian:  $SU(2) \times SU(2) \rightarrow SU(2)$ . In this case, one may parametrize as follows the leading-order terms in  $\mathcal{L}$ :

$$\begin{aligned}
\mathcal{L} = & \frac{v^2}{4} \text{Tr} D_\mu \Sigma^\dagger D^\mu \Sigma \left( 1 + 2a \frac{H}{v} + b \frac{H^2}{v^2} + \dots \right) \\
& - \bar{\psi}_L^i \Sigma \left( 1 + c \frac{H}{v} + \dots \right) \\
& + \frac{1}{2} (\partial_\mu H)^2 + \frac{1}{2} m_H^2 H^2 + d_3 \frac{1}{6} \left( \frac{3m_H^2}{v} \right) H^3 + d_4 \frac{1}{24} \left( \frac{3m_H^2}{v} \right) H^4 + \dots, \quad (11)
\end{aligned}$$

where

$$\Sigma \equiv \exp \left( i \frac{\sigma^a \pi^a}{v} \right). \quad (12)$$

The free coefficients  $a, b, c, d_3$  and  $d_4$  are all normalized such that they are unity in the SM, whereas composite models may give observable deviations from these values.

Fig. 9 shows the result of one analysis [23], that looked for possible rescalings of the  $H$  couplings to bosons by a factor  $a$  and to fermions by a factor  $c$ <sup>1</sup>. Clearly there is no sign of a significant deviation from the SM prediction  $a = c = 1$ , and the specific composite models shown as yellow lines in Fig. 9 are excluded unless (in some cases) their predictions can be adjusted to be very similar those of the SM.

### 3. The SM as an Effective Field Theory

In view of the continuing successes of the SM, now also in the Higgs sector, a common approach is to regard it as an effective field theory valid at low energies  $\lesssim 1$  TeV. The effects of higher-scale physics may then be expressed, as a first approximation, via higher-dimensional operators constructed out of SM fields, whose coefficients may be constrained by precision electroweak data, Higgs data and triple-gauge couplings (TGCs). Table 1 lists the operators entering electroweak

<sup>1</sup> For a similar recent result from the CMS Collaboration, see [11]. The ATLAS and CMS collaborations follow the Higgs Cross Section Working group in defining the quantities  $\kappa_V \equiv a$  and  $\kappa_f \equiv c$  [25].



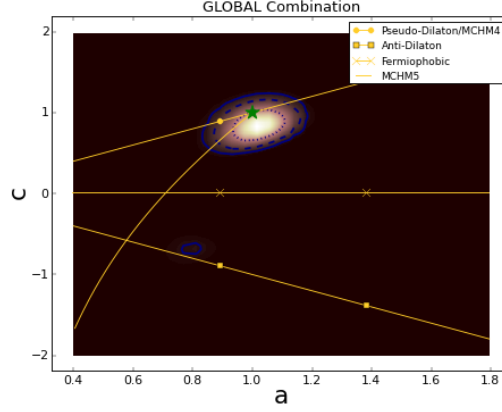


**Figure 9.** A global fit to bosonic and fermionic  $H$  couplings rescaled by factors  $a$  and  $c$ , respectively, indicating possible predictions of some composite models. The SM prediction  $a = c = 1$  is shown as the green star [23].

precision tests (EWPTs) at LEP, together with 95% CL bounds on their individual coefficients when they are switched on one at a time, and also when marginalised in a simultaneous global fit [26]. For the first four coefficients we list the constraints from the leptonic observables alone, while the constraints on the remaining coefficients also include hadronic observables.

Operator	Coefficient	LEP Constraints	
		Individual	Marginalized
$\mathcal{O}_W = \frac{ig}{2} (H^\dagger \sigma^a \leftrightarrow D^\mu H) D^\nu W_{\mu\nu}^a$ $\mathcal{O}_B = \frac{ig'}{2} (H^\dagger \leftrightarrow D^\mu H) \partial^\nu B_{\mu\nu}$	$\frac{m_W^2}{\Lambda^2} (c_W + c_B)$	$(-0.00055, 0.0005)$	$(-0.0033, 0.0018)$
$\mathcal{O}_T = \frac{1}{2} (H^\dagger \leftrightarrow D_\mu H)^2$	$\frac{v^2}{\Lambda^2} c_T$	$(0, 0.001)$	$(-0.0043, 0.0033)$
$\mathcal{O}_{LL}^{(3)l} = (\bar{L}_L \sigma^a \gamma^\mu L_L) (\bar{L}_L \sigma^a \gamma_\mu L_L)$	$\frac{v^2}{\Lambda^2} c_{LL}^{(3)l}$	$(0, 0.001)$	$(-0.0013, 0.00075)$
$\mathcal{O}_R^e = (iH^\dagger \leftrightarrow D_\mu H) (\bar{e}_R \gamma^\mu e_R)$	$\frac{v^2}{\Lambda^2} c_R^e$	$(-0.0015, 0.0005)$	$(-0.0018, 0.00025)$
$\mathcal{O}_R^u = (iH^\dagger \leftrightarrow D_\mu H) (\bar{u}_R \gamma^\mu u_R)$	$\frac{v^2}{\Lambda^2} c_R^u$	$(-0.0035, 0.005)$	$(-0.011, 0.011)$
$\mathcal{O}_R^d = (iH^\dagger \leftrightarrow D_\mu H) (\bar{d}_R \gamma^\mu d_R)$	$\frac{v^2}{\Lambda^2} c_R^d$	$(-0.0075, 0.0035)$	$(-0.042, 0.0044)$
$\mathcal{O}_L^{(3)q} = (iH^\dagger \sigma^a \leftrightarrow D_\mu H) (\bar{Q}_L \sigma^a \gamma^\mu Q_L)$	$\frac{v^2}{\Lambda^2} c_L^{(3)q}$	$(-0.0005, 0.001)$	$(-0.0044, 0.0044)$
$\mathcal{O}_L^q = (iH^\dagger \leftrightarrow D_\mu H) (\bar{Q}_L \gamma^\mu Q_L)$	$\frac{v^2}{\Lambda^2} c_L^q$	$(-0.0015, 0.003)$	$(-0.0019, 0.0069)$

**Table 1.** Operators and coefficients contributing to LEP electroweak precision tests (EWPTs), including 95% CL bounds when individual operators are switched on, and also when they are marginalised in a simultaneous global fit [26].

Our results for fits to the coefficients  $\bar{c}_{LL}^{(3)l}$ ,  $\bar{c}_T$ ,  $\bar{c}_W + \bar{c}_B$  and  $\bar{c}_R^e$  that affect the leptonic observables  $\{\Gamma_Z, \sigma_{\text{had}}^0, R_e^0, R_\mu^0, R_\tau^0, A_{\text{FB}}^{0,e}, m_W\}$  are shown in the left panel of Fig. 10. The upper (green) bars show the ranges for each of the coefficients varied individually, assuming that the other coefficients vanish, and the lower (red) bars show the ranges for a global fit in which all the coefficients are varied simultaneously. The legend at the top of the left panel of Fig. 10 translates the ranges of the coefficients into ranges of sensitivity to a large mass scale  $\Lambda$ . We see that all the sensitivities are in the multi-TeV range. The right panel of Fig. 10 shows the effect of including the hadronic observables  $\{R_b^0, R_c^0, A_{\text{FB}}^{0,b}, A_{\text{FB}}^{0,c}, A_b, A_c\}$ , and the operator coefficients



that contribute directly to them, namely  $\bar{c}_L^q, \bar{c}_L^{(3)q}, \bar{c}_R^u$  and  $\bar{c}_R^d$ .

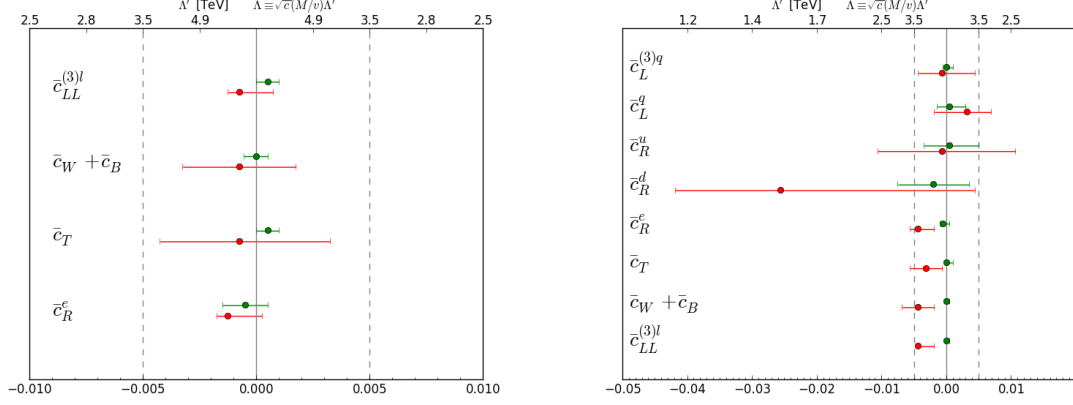


**Figure 10.** The 95% CL ranges found in analyses of the leptonic observables (left panel) and including also the hadronic observables (right panel). In each case, the upper (green) bars denote single-coefficient fits, and the lower (red) bars denote multi-coefficient fits. The upper-axis should be read  $\times \frac{m_W}{v} \sim 1/3$  for  $\bar{c}_W + \bar{c}_B$ . [26]

The operators with the largest effects on Higgs physics and TGCs are listed in Table 2<sup>2</sup>, together with 95% CL bounds obtained when individual operators are switched on one at a time, and also when they are marginalized in a simultaneous global fit [26]. Important information is provided by kinematic distributions [27], as well as by total rates, as seen in Fig. 11.

Operator	Coefficient	LHC Constraints	
		Individual	Marginalized
$\mathcal{O}_W = \frac{ig}{2} (H^\dagger \sigma^a \leftrightarrow D^\mu H) D^\nu W_{\mu\nu}^a$ $\mathcal{O}_B = \frac{ig'}{2} (H^\dagger \leftrightarrow D^\mu H) \partial^\nu B_{\mu\nu}$	$\frac{m_W^2}{\Lambda^2} (c_W - c_B)$	$(-0.022, 0.004)$	$(-0.035, 0.005)$
$\mathcal{O}_{HW} = ig (D^\mu H)^\dagger \sigma^a (D^\nu H) W_{\mu\nu}^a$	$\frac{m_W^2}{\Lambda^2} c_{HW}$	$(-0.042, 0.008)$	$(-0.035, 0.015)$
$\mathcal{O}_{HB} = ig' (D^\mu H)^\dagger (D^\nu H) B_{\mu\nu}$	$\frac{m_W^2}{\Lambda^2} c_{HB}$	$(-0.053, 0.044)$	$(-0.045, 0.075)$
$\mathcal{O}_{3W} = \frac{1}{3!} g \epsilon_{abc} W_\mu^{a\nu} W_\nu^b W_\rho^c W^{\rho\mu}$	$\frac{m_W^2}{\Lambda^2} c_{3W}$	$(-0.083, 0.045)$	$(-0.083, 0.045)$
$\mathcal{O}_g = g_s^2  H ^2 G_{\mu\nu}^A G^{A\mu\nu}$	$\frac{m_W^2}{\Lambda^2} c_g$	$(0, 3.0) \times 10^{-5}$	$(-3.2, 1.1) \times 10^{-4}$
$\mathcal{O}_\gamma = g'^2  H ^2 B_{\mu\nu} B^{\mu\nu}$	$\frac{m_W^2}{\Lambda^2} c_\gamma$	$(-4.0, 2.3) \times 10^{-4}$	$(-11, 2.2) \times 10^{-4}$

**Table 2.** List of operators entering in LHC Higgs and TGC physics, together with 95% CL bounds when individual coefficients are switched on one at a time, and marginalized in a simultaneous fit [26].

The results of a global fit to the Higgs data (including associated production kinematics) and LHC TGC measurements are summarised in Fig. 12 [26]. The individual 95% CL constraints obtained by switching one operator on at a time are shown as green bars. The other lines are the marginalised 95% ranges obtained using just the LHC signal-strength data in combination with the kinematic distributions for associated  $H + V$  production measured by ATLAS and D0 (blue bars), in combination with the LHC TGC data (red lines), and in combination with both

<sup>2</sup> EWPTs constrain the operators in Table 1 so strongly that they are not important for Higgs physics and TGCs.

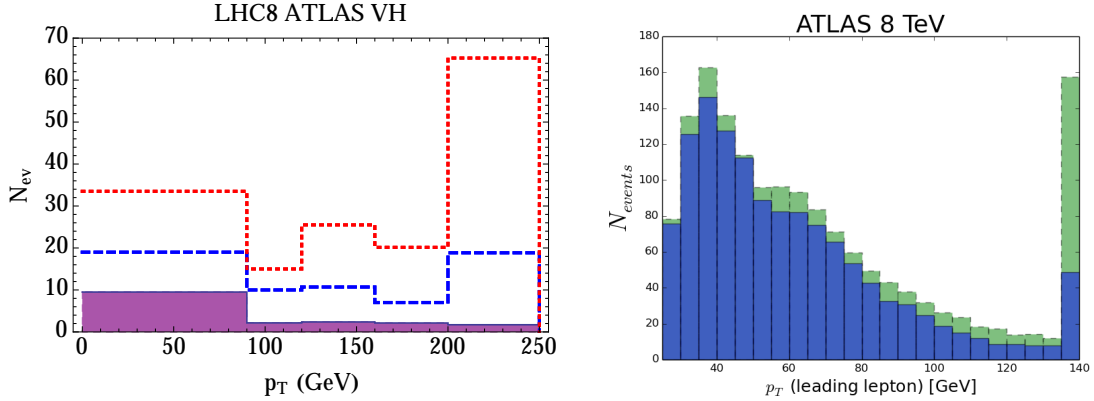


**Figure 11.** Left panel: Simulation of the  $p_T^V$  distribution in  $(V \rightarrow 2\ell) + (H \rightarrow \bar{b}b)$  events at the LHC after implementing ATLAS cuts. The solid distribution is the SM expectation, and the red-dotted and blue-dashed lines correspond to the distributions with  $\bar{c}_W = 0.1$  and  $0.05$ , respectively [27]. Right panel: The same-flavour  $p_T$  distribution of the leading lepton after the TGC analysis cuts for ATLAS at 8 TeV. The Standard Model distribution is shown in blue with solid lines, and the effect of  $\bar{c}_{HW} = 0.1$  is superimposed in green with dashed lines. In both cases the last (overflow) bin provides significant extra information compared to the overall normalisation [26].

the associated production and TGC data (black bars). We see that the LHC TGC constraints are the most important for  $\bar{c}_W$  and  $\bar{c}_{3W}$ , whereas the Higgs constraints are more important for  $\bar{c}_{HW}$ ,  $\bar{c}_{HB}$  and  $\bar{c}_g$ . Numerical results for the 95% CL ranges for these coefficients are shown alongside the operator definitions in Table 2.

#### 4. The SM is not enough!

Albert Michelson infamously asserted in 1894 that “*The more important fundamental laws and facts of physical science have all been discovered*”, just before the discoveries of radioactivity and the electron. Likewise, Lord Kelvin asserted in 1900 that “*There is nothing new to be discovered in physics now, all that remains is more and more precise measurement*”, just before Einstein postulated the photon and proposed special relativity. Even after the discovery of a (the?) Higgs boson, there are many reasons to expect physics beyond the SM, as I now discuss.

Inspired by James Bond [28], here are 007 of them. 1) The measured values of  $m_t$  and  $m_H$  suggest that the electroweak vacuum is *probably* unstable, unless some BSM physics intervenes. 2) The SM cannot provide the dark matter required by astrophysics and cosmology. 3) Additional CP violation beyond the CKM model is required to explain the origin of the matter in the Universe. 4) The small sizes of the neutrino masses seem to require BSM physics. 5) New physics at the TeV scale is needed for the hierarchy of mass scales to seem more natural. 6) BSM physics is required for cosmological inflation, notably because in the SM the effective Higgs potential would seem to become negative at high scales. 7) A consistent quantum theory of gravity would certainly require going (far) beyond the SM. Some of these issues are discussed in the following.

##### 4.1. The Instability of the Electroweak Vacuum

The effective electroweak potential of the SM resembles a Mexican hat, invariant under the SM  $SU(2) \times U(1)$  symmetry. The origin is unstable, and is surrounded by a valley where  $\langle H \rangle \equiv v = 246$  GeV, the electroweak vacuum. At larger Higgs field values, the brim of the

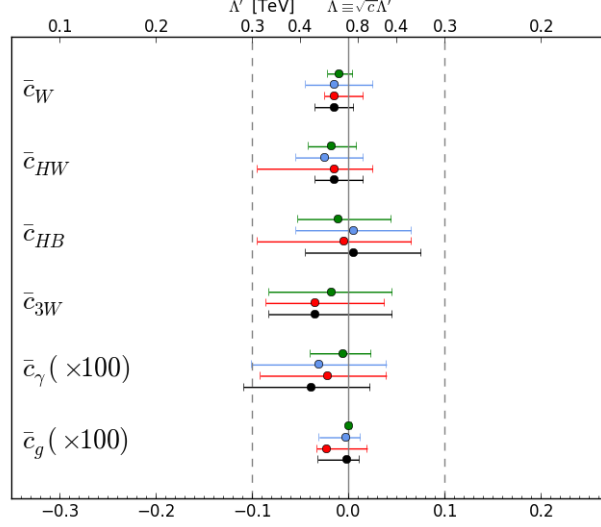


**Figure 12.** The 95% CL constraints obtained for single-coefficient fits (green bars), and the marginalised 95% ranges for the LHC signal-strength data combined with the kinematic distributions for associated  $H+V$  production measured by ATLAS and D0 (blue bars), combined with the LHC TGC data (red lines), and the global combination with both the associated production and TGC data (black bars). Note that  $\bar{c}_{\gamma,g}$  are shown  $\times 100$  for which the upper axis should therefore be read  $\times 10$  [26].

hat rises, at least for a while. However, calculations in the SM show that, for the measured values of  $m_t$  and  $m_H$  renormalization of the Higgs self-coupling by the top quark overwhelms that by the Higgs itself, turning the hat brim down at large field values. Thus, in the SM the present electroweak vacuum is unstable, in principle, with quantum tunnelling though the brim generating collapse into an anti-de-Sitter 'Big Crunch'.

According to the SM calculations [29] shown in the left panel of Fig. 13, the brim turns down at a Higgs scale  $\Lambda$ :

$$\log_{10} \left( \frac{\Lambda}{\text{GeV}} \right) = 11.3 + 1.0 \left( \frac{m_H}{\text{GeV}} - 125.66 \right) - 1.2 \left( \frac{m_t}{\text{GeV}} - 173.10 \right) + 0.4 \left( \frac{\alpha_s(M_Z) - 0.1184}{0.0007} \right). \quad (13)$$

Substituting the world average values of  $m_t$ ,  $m_H$  and  $\alpha_s(M_Z)$ , this formula yields

$$\Lambda = 10^{10.5 \pm 1.1} \text{ GeV}. \quad (14)$$

This calculation is very sensitive to  $m_t$ , as seen in the right panel of Fig. 13. The D0 Collaboration has recently reported a new, higher, value of  $m_t$  [30], which would tend to destabilise further the electroweak vacuum, whereas the CMS Collaboration has reported lower values of  $m_t$  from new analyses [31] that would tend to make the vacuum more stable. A more accurate experimental measurement of  $m_t$  would help us understand the fate of the Universe within the SM, but this experimental effort must be matched by improved understanding of the relationship between the parameter  $m_t$  in the SM Lagrangian and the effective mass parameter appearing in the Monte Carlos used by experiments [32].

According to these calculations, the lifetime of the electroweak vacuum would (probably) be much longer than the age of the Universe, but this does not mean that one can simply ignore

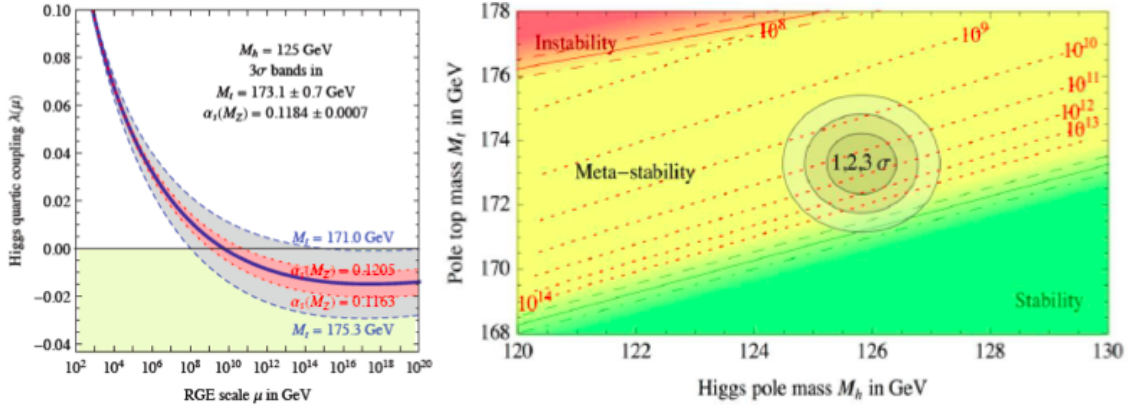


**Figure 13.** *Left panel: Within the SM, normalisation by the top quark appears to drive the Higgs self-coupling  $\lambda < 0$ . Right panel: The regions of vacuum stability, metastability and instability in the  $(m_H, m_t)$  plane. Both panels are from [29].*

the problem. We think that the Universe once had a very high energy density, e.g., during an inflationary epoch [33], and quantum and thermal fluctuations at that time would have tended to populate the anti-de-Sitter ‘Big Crunch’ region of the effective potential [34]. Of course, we might have struck lucky, living in a non-anti-de-Sitter region and thereby surviving - though this would require anthropic special pleading<sup>3</sup>. The problem could be avoided with suitable higher-dimensional terms in the effective potential [36], or other examples of new physics beyond the SM. One example is supersymmetry [37], which would have prevented the turn-down of the brim of the Mexican hat.

#### 4.2. Supersymmetry

There are many longstanding reasons for loving supersymmetry (SUSY), such as alleviating the fine-tuning aspect of the hierarchy problem, providing a natural candidate for the cold dark matter, facilitating grand unification and playing an essential rôle in string theory. Run 1 of the LHC has added three more reasons to this list, namely the mass of the Higgs boson, which is within the range predicted by supersymmetry [38, 39], the fact that the couplings resemble those of the SM Higgs boson, as expected in simple realisations of the minimal supersymmetric extension of the SM (MSSM) [40], and the stabilisation of the electroweak vacuum, as mentioned at the end of the previous Section. How could Nature resist SUSY’s manifold charms?

However, despite our ardent love for SUSY, so far she has kept out of sight. Direct searches for SUSY at the LHC have drawn blanks so far. This is also the case for searches for the scattering of dark matter particles, indirect searches in flavour physics, etc.. How can we interpret these searches, and where may SUSY be hiding? Unfortunately, we know that SUSY must be a broken symmetry, but we do not know how: there are no signposts in superspace! It is often assumed that there is a residual discrete R-symmetry that guarantees the stability of the lightest supersymmetric particle (LSP), which is the dark matter candidate mentioned above. Beyond that, it is often assumed (without much theoretical justification) that the SUSY-breaking sparticle masses are universal at some high renormalisation scale, usually the GUT scale. The simplest model in which all the SUSY-breaking contributions  $m_0$  to the squark, slepton and Higgs masses are equal at the GUT scale, and the SU(3), SU(2) and U(1) gauging masses  $m_{1/2}$  are also universal, is called the constrained MSSM (CMSSM). One may also consider models in which the SUSY-breaking contributions to the masses of the two Higgs doublets of the MSSM

<sup>3</sup> It has also been pointed out recently [35] that small black holes would catalyse rapid vacuum decay.

are equal but different from those of the squarks and leptons (the NUHM1), or where they are also different from each other (the NUHM2).

The results of global fits to the CMSSM, NUHM1 and NUHM2, combining all experimental and phenomenological constraints, and requiring that the relic supersymmetric particle density be within the cosmological range, are shown projected on the  $(m_0, m_{1/2})$  plane in the left panel of Fig. 14 [41, 42]. In these models the 95% CL lower limits on the squark and gluino masses are  $\sim 1.5$  GeV, as seen in Fig. 15. The right panel of Fig. 14 displays the corresponding  $(m_{\tilde{q}}, m_{\tilde{g}})$  plane, showing prospective exclusion and discovery reaches of the LHC in future runs with 300 and 3000/fb of luminosity at high energy [43]. Superposed on this plane are the 68 and 95% CL contours found in the global fit to the CMSSM. As already seen in the left panel of Fig. 14, there are two distinct regions, the lower-mass one being favoured by the disagreement between experiment and the SM prediction of  $g_\mu - 2$ . We see that future runs of the LHC could detect squarks and gluinos if Nature is described by supersymmetry with parameters in this lower-mass region of the CMSSM.

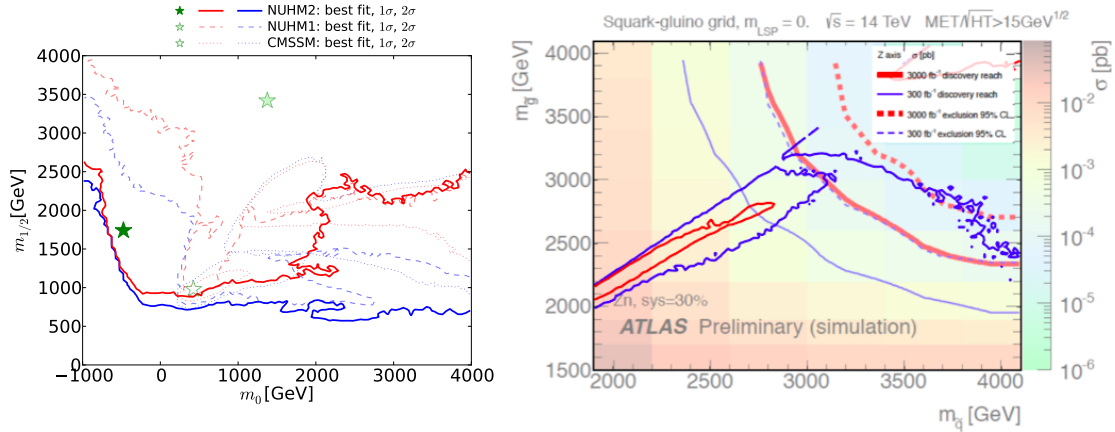


**Figure 14.** Left panel: The 68% CL (red) and 95% CL contours (blue) in the  $(m_0, m_{1/2})$  planes for the CMSSM (dotted lines), NUHM1 (dashed lines) and NUHM2 (solid lines) [42]. Right panel: The reach of ATLAS in the  $(m_{\tilde{q}}, m_{\tilde{g}})$  plane for exclusion and discovery with 300 and 3000/fb of integrated LHC luminosity at high energy [43], compared with the 68% CL (red) and 95% regions in the CMSSM.

One may, instead, consider the phenomenological MSSM (pMSSM) in which no universality is assumed. In this case, the lower limits on the gluino and squark masses are reduced, compared with the CMSSM, NUHM1 and NUHM2, as seen in Fig. 15, enhancing the prospects for discovering SUSY in LHC Run 2 [44]. The left panel of Fig. 15 displays the one-dimensional profile likelihood function for the mass of the gluino in the pMSSM, and the right panel is the corresponding plot for the first- and second-generation squarks.

The pMSSM offers anew the possibility that supersymmetry could explain the discrepancy between the SM calculation of  $g_\mu - 2$  and the experimental measurement. The LHC constraints on the CMSSM, NUHM1 and NUHM2 all predict values of the  $g_\mu - 2$  that are very similar to the unsuccessful SM prediction, as seen in the left panel of Fig. 16, whereas the experimental measurement pMSSM could be accommodated within the pMSSM [44]. Fortunately, there are plans for two new experiments to measure  $g_\mu - 2$  [45], and other low-energy  $e^+e^-$  experiments will help refine the SM predictions, clarifying the discrepancy between the SM and experiment. Turning to  $B_s \rightarrow \mu^+\mu^-$ , as seen in the right panel of Fig. 16, all of the CMSSM, NUHM1, NUHM2 and pMSSM predict branching ratios very similar to the SM.

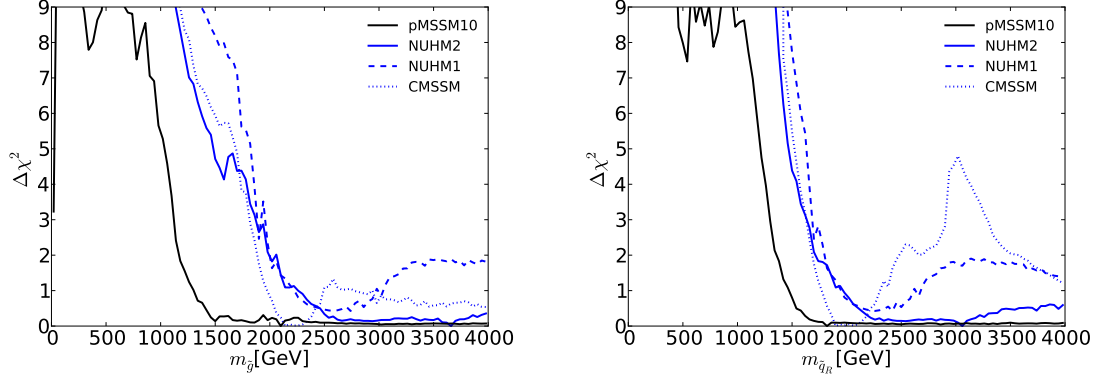


**Figure 15.** The one-dimensional profile likelihood functions for the gluino mass (left panel) and the first- and second-generation squark masses (right panel). In each panel the solid black line is for the pMSSM, the solid blue line for the NUHM2, the dashed blue line for the NUHM1 and the dotted blue line for the CMSSM [44].

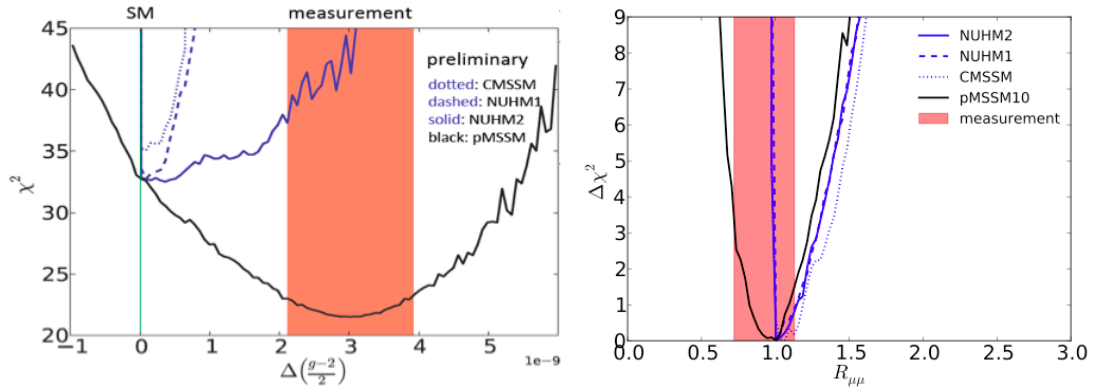


**Figure 16.** The one-dimensional  $\chi^2$  likelihood function for  $g_\mu - 2$  (left panel) and  $B_s \rightarrow \mu^+ \mu^-$  (right panel) in the CMSSM, NUHM1, NUHM2 and pMSSM [44]. The vertical shaded bands represent the 68% CL ranges of  $g_\mu - 2$  and  $B_s \rightarrow \mu^+ \mu^-$ .

## 5. CP-Violating MSSM Scenarios

In the CMSSM and related models, one can introduce 6 CP-violating phases, even if one assumes minimal flavour violation: there are 3 phases in the gaugino masses  $M_{1,2,3}$ , and 3 more in the third-generation trilinear SUSY-breaking couplings  $A_{t,b,\tau}$  [46]. There are 4 important constraints on these phases coming from upper limits on the electric dipole moments (EDMs) of the neutron, thorium monoxide, thallium and mercury. These 4 constraints in the 6-dimensional CP-violating parameter space leave a 2-dimensional blind subspace where combinations of the phases may be large, as seen in the case of the NUHM2 in Fig. 17 [47]. In the left panel we see the correlation these constraints impose between the phases of  $M_3$  and  $A_t$ , and in the right panel the correlation between the phases of  $M_3$  and  $A_b$ . In both cases we see diagonal features including populations of points with large phases: the EDM constraints do not require all the CP-violating phases to be small simultaneously.

We have explored what values of the CP-violating asymmetry in  $b \rightarrow s\gamma$  decays,  $A_{CP}$ , are compatible with the EDM constraints. We find that values of  $A_{CP} \lesssim 2\%$  can be found in the NUHM2 for values of the  $b \rightarrow s\gamma$  branching ratio lying within the experimentally-allowed range,



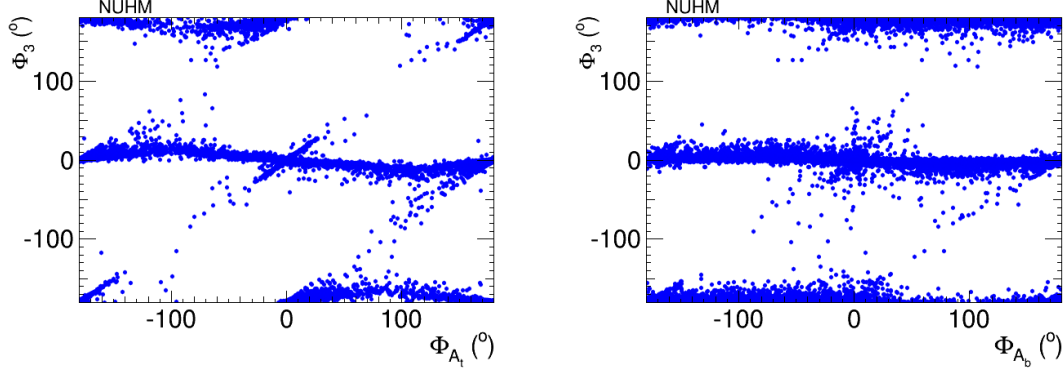


**Figure 17.** Correlations of the phase of  $M_3$  with that of  $A_t$  (left panel) and with that of  $A_b$  (right panel) imposed by the EDM constraints in the NUHM2 scenario [47].

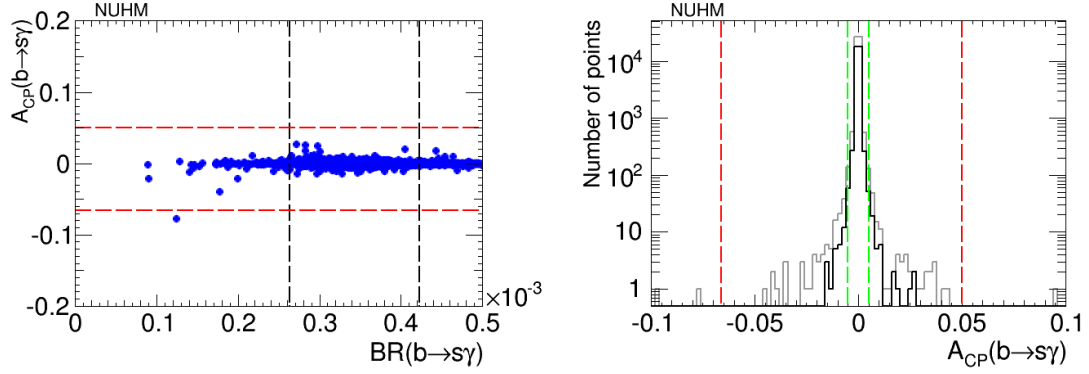


**Figure 18.** Left panel: Scatter plot of the branching ratio for  $b \rightarrow s\gamma$  decay versus its CP-violating asymmetry,  $A_{CP}$ , in the NUHM2 scenario. Right panel: Histogram of  $A_{CP}$  in the NUHM2, imposing only the Higgs mass and EDM cuts (grey: full sample, black: points satisfying the EDM constraints). The vertical red dashed lines represent the present experimental limits, and the vertical green dashed lines represent the prospective future improvement in the sensitivity to  $A_{CP}$  by a factor of ten [47].

as shown in the left panel of Fig. 18, and the right panel of this Figure displays a histogram of the NUHM2 results (grey: full sample, black: points satisfying the EDM constraints). The vertical red dashed lines are the present experimental constraints on  $A_{CP}$  [48]. According to a study of the prospective Belle II sensitivity [49], it should be possible to improve the present experimental sensitivity by a factor of ten, as shown by the vertical green dashed lines, and we see that there are some CP-violating NUHM2 models that could be explored with such an improvement. We conclude that the EDM constraints allow an observable value of  $A_{CP}$  within the NUHM2, and the same is true in the pMSSM.

## 6. Dark Matter Searches

As already commented, if a supersymmetric model conserves R-parity it provides a natural candidate for a cold dark matter particle. The same is true in some other TeV-scale extensions of the SM, such as some extra-dimensional models with K-parity and little Higgs models with



T-parity. The subject of searches for TeV-scale dark matter particles is vast, and there is no time or space here to discuss it in detail. However, I take the opportunity to display in Fig. 19 a recent comparison between the current reaches of the LHC via monojet searches and direct astrophysical searches for the scattering of generic TeV-scale dark matter particles, for the cases of spin-dependent (axial) couplings (left panel) and spin-independent (vector) couplings (right panel) [50]. We see that in the former case the LHC monojet searches generally have greater sensitivity than the direct searches, except for dark matter particle masses  $\gtrsim 1$  TeV where the LHC runs out of phase space. On the other hand, direct searches for spin-independent interactions are stronger than the LHC searches for masses  $\gtrsim 4$  GeV. Supersymmetry models generally favour a relatively large mass for the dark matter particle.

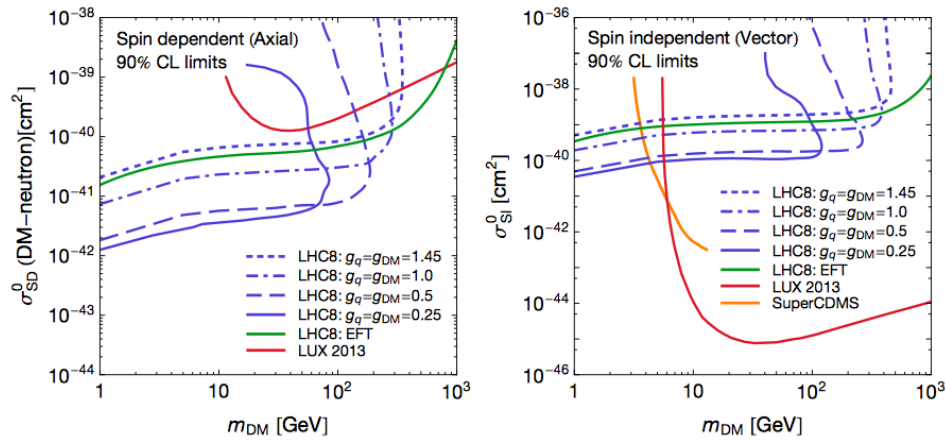


**Figure 19.** A comparison of the current 90% CL direct search limits from LUX and SuperCDMS (red and orange lines, respectively), the monojet limits in simple models (blue lines) and the limits in an effective field theory framework (green line) in the cross section vs  $m_{DM}$  plane used by the direct detection community. The left and right panels show, respectively, the limits on the spin-dependent and spin-independent cross sections appropriate for axial- vector and vector mediators [50].

## 7. Possible Future Colliders

In conclusion, here are a few words about possible future colliders. There has long been interest in building a high-energy linear  $e^+e^-$  collider such as the ILC ( $E_{CM} \lesssim 1$  TeV) or CLIC ( $E_{CM} \lesssim 3$  TeV), and there is now increasing interest in Europe and China in a possible large circular tunnel that could accommodate either an  $e^+e^-$  collider with  $E_{CM} \lesssim 350$  GeV and/or a  $pp$  collider with  $E_{CM} \lesssim 100$  TeV [51]. A circular  $e^+e^-$  collider could also provide unparalleled accuracy in measuring the properties of the  $Z$  and Higgs bosons, in particular, as seen in Fig. 20 [52]. In principle, these could be able to distinguish between the predictions of the SM and various fits in the CMSSM, NUHM1 and NUHM2, as shown. However, this will require considerable efforts to reduce correspondingly the present theoretical uncertainties, shown by the shaded green bars.

A future high-energy  $pp$  collider would also offer the possibility of producing very large numbers of Higgs bosons, as seen in the left panel of Fig. 21 [53], and studies are underway to estimate better the accuracies experiments could give in measuring Higgs couplings, including in particular the elusive triple-Higgs coupling, which will be very difficult to measure at the LHC or in any but a very high-energy  $e^+e^-$  collider. A high-energy  $pp$  collider would also offer unique possibilities to discover and/or measure the properties of supersymmetric particles. Even

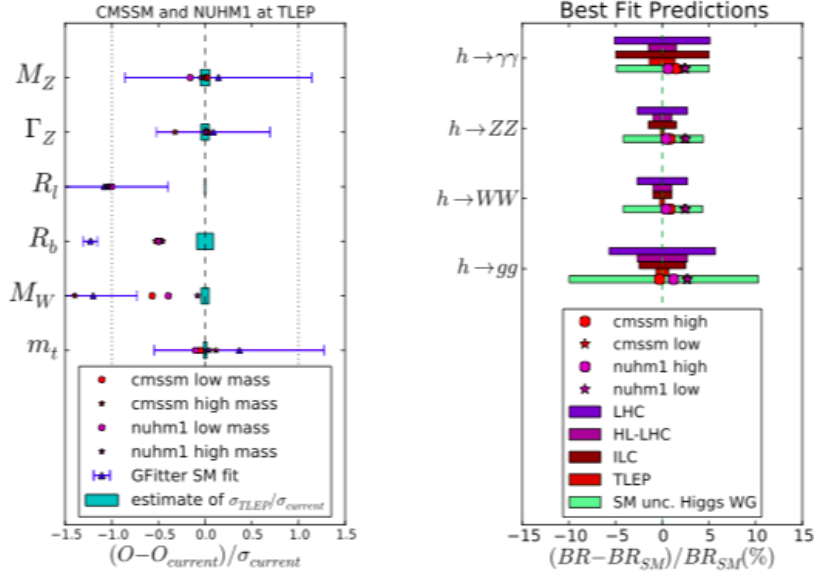


**Figure 20.** Comparison of the present precisions in measurements of various  $Z$  properties (left panel) and Higgs couplings (right panel), together with the prospective precisions of possible measurements at future colliders, the current theoretical uncertainties, and the deviations from the SM predictions found at the best-fit points in various SUSY models. From [52].

the lightest of these could weigh several TeV, as seen in the right panel of Fig. 21 [54]. In the example shown, only a  $pp$  collider with  $E_{\text{CM}} \sim 100$  TeV would be capable of exploring the full range of particle masses compatible with SUSY providing dark matter weighing  $\lesssim 3$  TeV (solid and upper dashed blue lines), and the green lines show that for all this range calculations of the Higgs mass are compatible with the experimental value (represented by the yellow band), considering the theoretical uncertainties represented by the green lines.

The physics cases for future large circular colliders are still to be developed. Certainly there will be a strong bedrock of high-precision Higgs and other SM measurements to test possible scenarios for physics beyond the SM. As for direct searches for new physics, the search for dark matter particles looks to provide the strongest case, but this still requires further study. Needless to say, the physics landscape will look completely different when/if future runs of the LHC at higher energy and luminosity provide some evidence for new physics beyond the SM. Some of my supersymmetric friends are disappointed that SUSY has not shown up yet, but the LHC saga has only just begun. It took 48 years for the Higgs boson to be discovered [55] (the record time-lag so far), but four-dimensional supersymmetric were first written down only 41 years ago [56], so let us be patient for a while longer!

## Acknowledgments

I am grateful to Nick Mavromatos and Sarben Sarkar for their kind invitation to speak at this fun conference. The work was supported in part by the London Centre for Terauniverse Studies (LCTS), using funding from the European Research Council via the Advanced Investigator Grant 267352 and from the UK STFC via the research grant ST/J002798/1.

## References

- [1] CMS Collaboration, <https://twiki.cern.ch/twiki/bin/view/CMSPublic/PhysicsResultsSMP>.
- [2] G. Aad *et al.* [ATLAS Collaboration], Phys. Lett. B **716** (2012) 1 [arXiv:1207.7214 [hep-ex]]; S. Chatrchyan *et al.* [CMS Collaboration], Phys. Lett. B **716** (2012) 30 [arXiv:1207.7235 [hep-ex]].

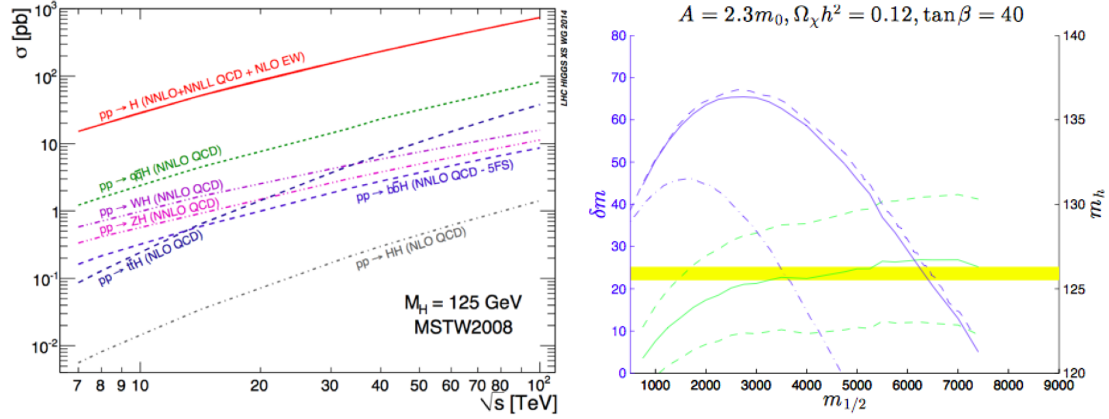


**Figure 21.** Left panel: Cross sections for various Higgs production processes at  $pp$  colliders as functions of the centre-of-mass energy [53]. Right panel: One of the possibilities for a relatively heavy supersymmetric dark matter particle weighing  $\sim 0.4m_{1/2} \lesssim 3$  TeV. The vertical axis is the mass difference between the dark matter particle and the next-to-lightest supersymmetric particle, in this case the lighter stop squark. The solid and upper dashed blue lines correspond to the current central and  $+1\sigma$  values of the dark matter density, the horizontal yellow band represents the experimental value of the Higgs mass, and the green lines represent the central value and  $\pm 1\sigma$  uncertainties in theoretical calculations of the Higgs mass [54].

- [3] J. Charles, O. Deschamps, S. Descotes-Genon, H. Lacker, A. Menzel, S. Monteil, V. Niess and J. Ocariz *et al.*, arXiv:1501.05013 [hep-ph].
- [4] V. Khachatryan *et al.* [CMS and LHCb Collaborations], arXiv:1411.4413 [hep-ex] and references therein.
- [5] R. Aaij *et al.* [LHCb Collaboration], Phys. Rev. Lett. **113** (2014) 151601 [arXiv:1406.6482 [hep-ex]].
- [6] R. Aaij *et al.* [LHCb Collaboration], Phys. Rev. Lett. **111** (2013) 19, 191801 [arXiv:1308.1707 [hep-ex]].
- [7] CMS Collaboration, <https://cds.cern.ch/record/1740976?ln=en>.
- [8] V. M. Abazov *et al.* [D0 Collaboration], Phys. Rev. Lett. **105** (2010) 081801 [arXiv:1007.0395 [hep-ex]].
- [9] T. Aaltonen *et al.* [CDF Collaboration], Phys. Rev. D **87** (2013) 9, 092002 [arXiv:1211.1003 [hep-ex]].
- [10] G. Aad *et al.* [ATLAS Collaboration], Phys. Rev. D **90** (2014) 052004 [arXiv:1406.3827 [hep-ex]].
- [11] V. Khachatryan *et al.* [CMS Collaboration], arXiv:1412.8662 [hep-ex].
- [12] G. Aad *et al.* [ATLAS Collaboration], Phys. Lett. B **726** (2013) 120 [arXiv:1307.1432 [hep-ex]].
- [13] V. Khachatryan *et al.* [CMS Collaboration], arXiv:1411.3441 [hep-ex].
- [14] T. A. Aaltonen *et al.* [CDF Collaboration], arXiv:1501.04875 [hep-ex].
- [15] J. Ellis, V. Sanz and T. You, Phys. Lett. B **726** (2013) 244 [arXiv:1211.3068 [hep-ph]].
- [16] J. Ellis, D. S. Hwang, V. Sanz and T. You, JHEP **1211** (2012) 134 [arXiv:1208.6002 [hep-ph]].
- [17] J. Ellis, R. Fok, D. S. Hwang, V. Sanz and T. You, Eur. Phys. J. C **73** (2013) 2488 [arXiv:1210.5229 [hep-ph]], and references therein.
- [18] A. Askew, P. Jaiswal, T. Okui, H. B. Prosper and N. Sato, arXiv:1501.03156 [hep-ph], and references therein.
- [19] J. Ellis, D. S. Hwang, K. Sakurai and M. Takeuchi, JHEP **1404** (2014) 004 [arXiv:1312.5736 [hep-ph]].
- [20] ATLAS Collaboration, <https://twiki.cern.ch/twiki/bin/view/AtlasPublic/HiggsPublicResults>.
- [21] S. Chatrchyan *et al.* [CMS Collaboration], JHEP **1306** (2013) 081 [arXiv:1303.4571 [hep-ex]].
- [22] CDF and D0 Collaborations, <http://tevnpnphwg.fnal.gov>.
- [23] J. Ellis and T. You, JHEP **1306** (2013) 103 [arXiv:1303.3879 [hep-ph]]. References to the original literature can be found here.
- [24] G. Blankenburg, J. Ellis and G. Isidori, Phys. Lett. B **712** (2012) 386 [arXiv:1202.5704 [hep-ph]].
- [25] A. David *et al.* [LHC Higgs Cross Section Working Group Collaboration], arXiv:1209.0040 [hep-ph].
- [26] J. Ellis, V. Sanz and T. You, arXiv:1410.7703 [hep-ph]. References to the original literature can be found here.
- [27] J. Ellis, V. Sanz and T. You, JHEP **1407** (2014) 036 [arXiv:1404.3667 [hep-ph]].
- [28] J. Bond *et al.*, <http://www.imdb.com/title/tt0143145/>.
- [29] D. Buttazzo, G. Degrandi, P. P. Giardino, G. F. Giudice, F. Sala, A. Salvio and A. Strumia, JHEP **1312**

- (2013) 089 [arXiv:1307.3536].
- [30] A. Jung, on behalf of the D0 Collaboration, <https://indico.cern.ch/event/279518/session/27/contribution/36/material/slides/0.pdf>.
  - [31] CMS Collaboration, <http://cds.cern.ch/record/1951019/files/TOP-14-015-pas.pdf>.
  - [32] S. Moch, S. Weinzierl, S. Alekhin, J. Blumlein, L. de la Cruz, S. Dittmaier, M. Dowling and J. Erler *et al.*, arXiv:1405.4781 [hep-ph].
  - [33] P. A. R. Ade *et al.* [Planck Collaboration], Astron. Astrophys. **571** (2014) A22 [arXiv:1303.5082 [astro-ph.CO]]; P. A. R. Ade *et al.* [BICEP2 Collaboration], Phys. Rev. Lett. **112** (2014) 241101 [arXiv:1403.3985 [astro-ph.CO]].
  - [34] M. Fairbairn and R. Hogan, Phys. Rev. Lett. **112** (2014) 201801 [arXiv:1403.6786 [hep-ph]]; A. Hook, J. Kearney, B. Shakya and K. M. Zurek, arXiv:1404.5953 [hep-ph].
  - [35] P. Burda, R. Gregory and I. Moss, arXiv:1501.04937 [hep-th].
  - [36] V. Branchina, E. Messina and M. Sher, arXiv:1408.5302 [hep-ph].
  - [37] J. R. Ellis and D. Ross, Phys. Lett. B **506** (2001) 331 [hep-ph/0012067].
  - [38] J. R. Ellis, G. Ridolfi and F. Zwirner, Phys. Lett. B **257** (1991) 83; H. E. Haber and R. Hempfling, Phys. Rev. Lett. **66** (1991) 1815; Y. Okada, M. Yamaguchi and T. Yanagida, Prog. Theor. Phys. **85** (1991) 1.
  - [39] T. Hahn, S. Heinemeyer, W. Hollik, H. Rzehak and G. Weiglein, Phys. Rev. Lett. **112** (2014) 14, 141801 [arXiv:1312.4937 [hep-ph]].
  - [40] J. R. Ellis, S. Heinemeyer, K. A. Olive and G. Weiglein, Phys. Lett. B **515** (2001) 348 [hep-ph/0105061].
  - [41] O. Buchmueller, R. Cavanaugh, A. De Roeck, M. J. Dolan, J. R. Ellis, H. Flacher, S. Heinemeyer and G. Isidori *et al.*, Eur. Phys. J. C **74** (2014) 6, 2922 [arXiv:1312.5250 [hep-ph]].
  - [42] O. Buchmueller, R. Cavanaugh, M. Citron, A. De Roeck, M. J. Dolan, J. R. Ellis, H. Flaecher and S. Heinemeyer *et al.*, arXiv:1408.4060 [hep-ph].
  - [43] ATLAS Collaboration, arXiv:1307.7292 [hep-ex].
  - [44] O. Buchmueller, R. Cavanaugh, M. Citron, A. De Roeck, M. J. Dolan, J. R. Ellis, H. Flaecher and S. Heinemeyer *et al.*, *The pMSSM after LHC Run 1*, in preparation.
  - [45] FNAL g-2 Collaboration, <http://muon-g-2.fnal.gov>; H. Inuma (for the J-PARC New g-2/EDM experiment Collaboration), [http://iopscience.iop.org/1742-6596/295/1/012032/pdf/1742-6596\\_295\\_1\\_012032.pdf](http://iopscience.iop.org/1742-6596/295/1/012032/pdf/1742-6596_295_1_012032.pdf).
  - [46] J. R. Ellis, J. S. Lee and A. Pilaftsis, Phys. Rev. D **76** (2007) 115011 [arXiv:0708.2079 [hep-ph]]; JHEP **1010** (2010) 049 [arXiv:1006.3087 [hep-ph]].
  - [47] A. Arbey, J. Ellis, R. M. Godbole and F. Mahmoudi, arXiv:1410.4824 [hep-ph].
  - [48] K. A. Olive *et al.* [Particle Data Group Collaboration], Chin. Phys. C **38** (2014) 090001.
  - [49] T. Aushev, W. Bartel, A. Bondar, J. Brodzicka, T. E. Browder, P. Chang, Y. Chao and K. F. Chen *et al.*, arXiv:1002.5012 [hep-ex].
  - [50] O. Buchmueller, M. J. Dolan, S. A. Malik and C. McCabe, JHEP **1501** (2015) 037 [arXiv:1407.8257 [hep-ph]]; S. Malik, C. McCabe, H. Araujo, A. Belyaev, C. Boehm, J. Brooke, O. Buchmueller and G. Davies *et al.*, arXiv:1409.4075 [hep-ex].
  - [51] <https://espace2013.cern.ch/fcc/Pages/default.aspx>.
  - [52] M. Bicer *et al.* [TLEP Design Study Working Group Collaboration], JHEP **1401** (2014) 164 [arXiv:1308.6176 [hep-ex]].
  - [53] LHC Higgs Cross-Section Working Group, as reported in M. Klute, <http://indico.cern.ch/event/300048/session/13/contribution/60/material/slides/0.pdf>.
  - [54] J. Ellis, K. A. Olive and J. Zheng, Eur. Phys. J. C **74** (2014) 2947 [arXiv:1404.5571 [hep-ph]].
  - [55] <http://www.economist.com/blogs/graphicdetail/2012/07/daily-chart-1>.
  - [56] J. Wess and B. Zumino, Phys. Lett. B **49** (1974) 52.